ACS OMEGA

http://pubs.acs.org/journal/acsodf

Article

Gentamycin Rationally Repositioned to Inhibit miR-34a Ameliorates Oxidative Injury to PC12 Cells

Zhila Izadi, Ebrahim Barzegari, Amin Iranpanah, Soraya Sajadimajd,* and Hossein Derakhshankhah*

Cite This: *ACS Omega* 2023, 8, 771−781

Read Online

ACCESS | Metrics & More | Article Recommendations | Supporting Information

ABSTRACT: Ischemic stroke accompanies oxidative stress and cell death in the cerebral tissue. The microRNA miR-34a plays a pivotal role in this molecular pathology. This study presents the rational repositioning of aminoglycosidic antibiotics as miR-34a antagonists in order to assess their efficiency in protecting the PC12 stroke model cells from oxidative stress occurring under cerebral ischemic conditions. A library of 29 amino-sugar compounds were screened against anticipated structural models of miR-34a through molecular docking. MiR−ligand interactions were mechanistically studied by molecular dynamics simulations and free-energy calculations. Cultured PC12 cells were treated by H_2O_2 alone or in combination with gentamycin and neomycin as selected drugs. Cell viability and apoptosis were detected by 3-(4,5-dimethylthiazolyl-2)-2,5-diphenyltetrazolium bromide (MTT) and annexin V-FITC/propidium iodate (PI) double staining assays, respectively. The expression levels of key factors involved in cell proliferation, oxidative stress, and apoptosis in treated PC12 cells were measured through a quantitative real-time polymerase chain reaction and flow cytometric annexin V-FITC/PI double staining assays. A stable and energetically favorable binding was observed for miR-34a with gentamycin and neomycin. Gentamycin pretreatments followed by H_2O_2 oxidative injury led to increased cell viability and protected PC12 cells against H_2O_2-induced apoptotic events. This study will help in further understanding how the suppression of miR-34a in neural tissue affects the cell viability upon stroke.

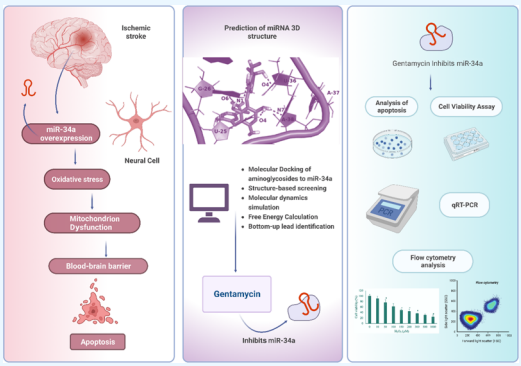

INTRODUCTION

Stroke, the second leading cause of death worldwide,[1−4] is a major cause of long-term disability, which diminishes the quality of life of patients and imposes heavy lifetime costs per person for patients and the healthcare system.[2,4−7] This cerebrovascular condition is clinically defined as the sudden loss of focal neurological function which occurs due to ischemia or hemorrhage in the brain, retina, or spinal cord.[8] Cerebral ischemia, which mainly occurs due to embolism or thrombosis, sets off a cascade of events which includes disturbance of membrane function with calcium influx, generation of reactive oxygen species, and ultimately destruction of cell membranes and cell lysis.[6] Thus, hypoxia and the resulting oxidative stress play a critical role in promoting the pathogenesis and all the outcomes presenting poststroke.[9−12]

MicroRNAs (miRNAs; miRs) are an important class of noncoding and regulatory single-stranded RNAs. The biogenesis of miRNAs includes their transcription by RNA polymerase II, shortening by the enzyme Drosha, cleavage of the loop by the dicer, unwinding, and maturation. The mature miRNA restricts the expression of its target gene(s) by complementary binding to the 3′-UTR region of its messenger RNA. The discovery of miRNAs offered a breakthrough in the approach to the pathogenesis and management of many challenging diseases of humans.[13−15]

MicroRNA-34a (miR-34a) has been identified as a tumor-suppressing miR with a central role in the pathways and feedback loops orchestrating both cell proliferation and death under physiological or pathological conditions.[16,17] Given the key contribution of this miRNA to cell growth, its pivotal modulatory potential in neurological disorders, including in the hypoxic stress-induced apoptosis in stroke, is evident.[18] Furthermore, the overexpression of miR-34a has been demonstrated to break down the blood−brain barrier (BBB) by suppressing mitochondrial function.[19,20] The microRNA targets the electron transport chain protein, cytochrome *c*, which impairs the mitochondrial oxidative phosphorylation and leads to the disruption of tight junctions of cerebrovascular endothelial cells.[19] The compromised BBB integrity and permeability cause the opening of the BBB and the exacerbation of stroke outcomes.[20,21] In general, elevated levels of miR-34a during ischemic stroke contribute to neuronal injury and death,

Received: September 22, 2022
Accepted: December 8, 2022
Published: December 16, 2022

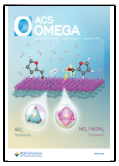

while suppression of its levels may be generally neuroprotective.[18] Therefore, the modulation of miR-34a expression or function is expected to result in altered outcomes of stroke.[22]

By applying the knowledge available in the area of miRNA inhibition, in this study, we aim to design appropriate antagonists for miR-34a and assay their efficiency in protecting the neurological cell model (PC12 cells) from the oxidative injury characteristic of ischemic cerebrovascular diseases. Recent studies tend to employ small molecules to block miRNA maturation. Such therapeutics provide several advantages over antagomirs and peptide anti-miRs, including higher molecular stability and more efficient delivery to tissues.[23,24] Aminoglycosides are a kind of small molecules, which are known to bind to RNA secondary structures.[23,25] Here, we used rational screenings and molecular mechanistic investigations to identify an amino sugar to target miR-34a. Additionally, the bottom-up approach in miR antagonism is considered to detect high-specificity leads for miR-34a.[26] We then analyzed the effects of the top lead compounds and their combination treatments with H_2O_2 on cell viability loss, proliferation inhibition, oxidative stress increase, and apoptosis in the PC12 model of oxidative injury in ischemic stroke. The expression levels of key factors involved in cell proliferation, oxidative stress, and apoptosis are evaluated in treated PC12 cells.

MATERIALS AND METHODS

Prediction of the miRNA 3D Structure. The stem-loop sequence of rat pre-miR-34a (rno-mir-34a) was obtained from miRbase (www.mirbase.org; accession number: MI0000877). The rat species was selected to allow the results to be exploited in wet lab experiments using PC12 rat cells. In the next step, the tertiary structure of miR-34a was predicted using the MC pipeline.[27] The tool allows RNA secondary structure prediction from the sequence by MC-fold, followed by tertiary structure prediction from the secondary one by MC-Sym. MC-fold is a knowledge-based platform attempting to integrate the in-stem noncanonical base pairs into a unified energetic framework. It derives a pseudopotential energy function for nucleotide cyclic motifs obtained from the Protein Data Bank. MC-Sym then fuses the cyclic motifs to generate models of tertiary structures. The models' quality is shown by the structure energies and the proposed *P*-score of the program.

A sequence region of the miRNA encompassing nucleotides 26−85 (60 nucleotides), which contained the hairpin loop region was selected as the query to make the 3D model of miR-34a. We considered two model productions using two different secondary structures proposed for miR-34a. The first modeling type utilized the secondary structure predicted by MC-Fold from the raw sequence. In the second one, we assumed the secondary structure from the general annotation of miR-34a as determined by deep sequencing and large-scale characterizations, presented in miR repositories.

Molecular Docking of Aminoglycosides to miR-34a. A library of 29 compounds with an aminoglycosidic structure, most of which are generic FDA-approved antibiotics, were collected from the literature (Figure S1). The chemical structures were retrieved from PubChem or DrugBank and underwent energy optimization by using the MM2 method implemented in the ChemOffice suite. These ligands were docked to either of the miRNA structural models as receptors. The Autodock program was employed for molecular dockings. The dicer-binding region on pre-miRNA-34a was defined as the suitable binding site of the small molecules. The docking search space was set to only cover the hairpin loop and nearby residues. After adding Gasteiger charges to the ligand, a Lamarckian genetic algorithm and an empirical binding free-energy function were employed for automated docking using the AutoDock-Tools 4.2 software. For each selected molecule, trials of 10 dockings and 2,500,000 energy evaluations were performed. Only hydrogen bonds (H-bonds) with a length of <0.35 nm and an α angle of $\leq 30^\circ$ between the cooperated donor and acceptor heavy atoms were taken into account.

Structure-Based Screening. We set up a virtual screening to examine whether compounds with structural similarity to aminoglycosides known as top-most compound hits at the preceding step could bind and inhibit miR-34a processing with stronger interaction than the corresponding aminoglycosides. By exploring the compounds in the ZINC database of over 230 million chemicals, we retrieved 30 of the most similar analogues of the ligand queries. The chemical structures were then optimized by energy minimization using the MM2 method. Following that, the docking process for the amino-sugar analogues was carried out in the same manner as in the previous step. Eventually, the compounds with the lowest binding energy were identified and compared to the original aminoglycosides.

Molecular Dynamics Simulation. Based on the results from the docking section, the most promising RNA−ligand complex was chosen as the initial coordinate to carry out molecular dynamics (MD) simulations comparatively with the ligand-free miR molecule. Simulation trajectories were produced using GROMACS-5.1.2 software, applying the AMBER-99 force field.[28] The ACPYPE server was utilized for generating the ligand topology.[29] The miRNA−ligand complex was placed in the center of a cubic box. An explicit SPC/E water model was used for solvation. A sufficient number of Na^+ ions were added to the system for neutralizing the negative charges on phosphate groups of the RNA backbone. Prior to the product simulations, the system underwent a maximum of 50,000 steps of steepest-descent energy minimization until the energy gradient was smaller than 1000.0 kJ/mol/nm. The linear constraint (LINCS) algorithm was applied to fix all hydrogen-related bond lengths, facilitating the use of a 2 fs time step. To treat long-range electrostatic interactions, we employed the particle mesh Ewald algorithm. The bond lengths involving H-atoms were constrained using the SHAKE algorithm. The energy minimization was followed by equilibration for 200 ps with each of the *NVT* and *NPT* ensembles. Eventually, the production run for the system with a constant temperature of 300 K and a constant pressure of 1 bar was implemented to simulate the systems' behavior for 60 ns. Gromacs and PyMol (www.pymol.org) were used for analyzing output data.

Free-Energy Calculations. The molecular mechanics/Poisson-Boltzmann surface area (MM/PBSA) method was utilized to calculate the free-energy change upon ligand binding. The $\Delta G_{binding}$ can be decomposed into an intermolecular interaction potential ΔE_{MM} between RNA and the ligand and a desolvation penalty ΔG_{PBSA} due to the stripping of water molecules from the interaction interface. The desolvation can be divided into polar (electrostatic; ΔG_{PB}) and nonpolar (van der Waals; ΔG_{SA}) contributions. These calculations were run using the g_mmpbsa tool.[30]

Bottom-Up Lead Identification. Disney et al. proposed a method to identify the small-molecule modifiers of miRNAs through the prediction of lead compounds based on experimentally derived parameters to directly target miRNAs. The method incorporated a two-dimensional combinatorial

https://doi.org/10.1021/acsomega.2c06112
ACS Omega 2023, 8, 771−781

Table 1. Sequence of Primers used for qRT-PCR

gene	oligonucleotide sequence	
	forward (5′-3′)	reverse (5′-3′)
P53	CATCATCACGCTGGAAGACTC	GGACAGGCACAAACACGAAC
SIRT1	AAGACCAGTAGCACTAATTCCAAGT	AAGACCAGTAGCACTAATTCCAAGT
Caspase-3	GTGGAACTGACGATGATATGG	GCAAAGTGACTGGATGAACC
β-actin	TGACCCAGATCATGTTTGAGACC	CTCATAGATGGGCACAGTGTGGG
rno-miR34a-5p stem loop	GTCGTATCCAGTGCAGGGTCCGAGGTATTCGCACTGGATACGACACAACCA	
rno-miR34a-5p	AATCGGCGTGGCAGTGTCTTA	GTCGTATCCAGTGCAGGGTCC
u6 snRNA stem-loop	AACGCTTCACGAATTTGCGTG	
u6 snRNA	GCTCGCTTCGGCAGCACA	GAGGTATTCGCACCAGAGGA

Table 2. Docking Energies for the Aminoglycosidic Ligands Bound to miR-34a Structural Models

ligand	model-1		model-2	
	binding energy (kcal/mol)	inhibition constant (nM)	binding energy (kcal/mol)	inhibition constant (nM)
amikacin	0.81	N.A.	−2.08	3.0×10^{7}
apramycin	−13.89	6.62×10^{-2}	−16.38	9.85×10^{-4}
arbekacin	−10.28	29.1	−15.91	2.17×10^{-3}
astromicin	−11.74	2.49	−14.11	4.51×10^{-2}
bekanamycin	−11.34	4.89	−14.6	2.0×10^{-2}
butirosin A	−9.61	90.4	−10.66	15.3
dibekacin	−12.54	6.44×10^{-1}	−15.82	2.55×10^{-3}
dihydrostreptomycin	−7.27	4.71×10^{3}	−10.52	19.4
framycetin	−11.68	2.75	−16.77	5.10×10^{-4}
G418	−9.37	1.36×10^{2}	−13.64	1.01×10^{-1}
gentamicin	−12.4	8.18×10^{-1}	−16.24	1.25×10^{-3}
gentamycin C1	−13.46	1.36×10^{-1}	−17.89	7.76×10^{-5}
hygromycin B	−7.85	1.75×10^{3}	−11.22	6.0
isepamicin	−10.03	44.5	−12.04	1.51
kanamycin	−11.24	5.74	−12.74	4.56×10^{-1}
kanamycin2	−9.65	84.5	−12.3	9.57×10^{-1}
neomycin C	−12.24	1.07	−17.12	2.82×10^{-4}
neomycin C2	−10.69	14.6	−14.53	2.23×10^{-2}
netilmicin	−12.83	3.94×10^{-1}	−17.25	2.26×10^{-4}
nourseothricin	−8.49	5.96×10^{2}	−11.5	3.74
paromomycin	−9.52	1.05×10^{2}	−13.61	1.05×10^{-1}
plazomicin	−10.15	36.3	−14.35	3.04×10^{-2}
puromycin	−7.08	6.44×10^{3}	−6.42	1.98×10^{4}
ribostamycin	−9.72	75.5	−12.51	6.71×10^{-1}
sisomicin	−13.01	2.90×10^{-1}	−17.05	3.17×10^{-4}
spectinomycin	−8.98	2.62×10^{2}	−10.2	33.1
streptomycin	−8.44	6.56×10^{2}	−10.33	27.0
tobramycin	−13.16	2.24×10^{-1}	−14.88	1.24×10^{-2}
verdamicin	−13.14	2.35×10^{-1}	−16.25	1.25×10^{-3}

screening to identify ligands that made specific binding to RNA secondary structural motifs (bulges or loops). Then, features of RNA-motif small-ligand interactions, including both affinity and selectivity, were determined using a statistical fitness score, and the data were deposited in Inforna, the specific repository for such information.[26,31] We submitted our miRNA model-2 data to Inforna and selected leads from among output hits considering features of motif−ligand interactions.

Cell Culture and Treatments. Rat PC12 cells, provided by the National Cell Bank of Iran, were cultured in a Roswell Park Memorial Institute (RPMI) 1640 medium supplemented with 10% fetal bovine serum and 100 U/mL penicillin in a humidified 5% CO_2 atmosphere at 37 °C (sixth passage number of cell lines). Drug treatment was commonly performed 24 h after seeding the cells. Freshly prepared H_2O_2 in phosphate-buffered saline (PBS) was used to induce oxidative stress. Gentamycin (Gen; G) and neomycin (Neo; N) stock solutions (1 mg/mL) were prepared in the culture medium.

Cell Viability Assay. The cytotoxicity of each drug was evaluated by the MTT assay as described by Vistica et al.[32] In brief, PC12 cells at a density of 5×10^{3}/well were seeded into 96-well plates for 24 h and then treated either with each drug alone (H_2O_2, gentamycin, and neomycin) or in combination. Treated cells were incubated at 37 °C for the indicated time intervals. Then, the media were replaced and 10 μL of MTT (5 mg/mL) was added to each well. Following 4 h of incubation, the media were discarded and DMSO (100 μL) was added to each well for dissolving the formazan crystals. Afterward, the viability of cells was evaluated by measuring the absorbance at 570 nm using an ELISA reader (BioTek Synergi H1 microplate reader). The values were expressed as mean ± standard deviation (SD) of at least three independent experiments,

https://doi.org/10.1021/acsomega.2c06112
ACS Omega 2023, 8, 771−781

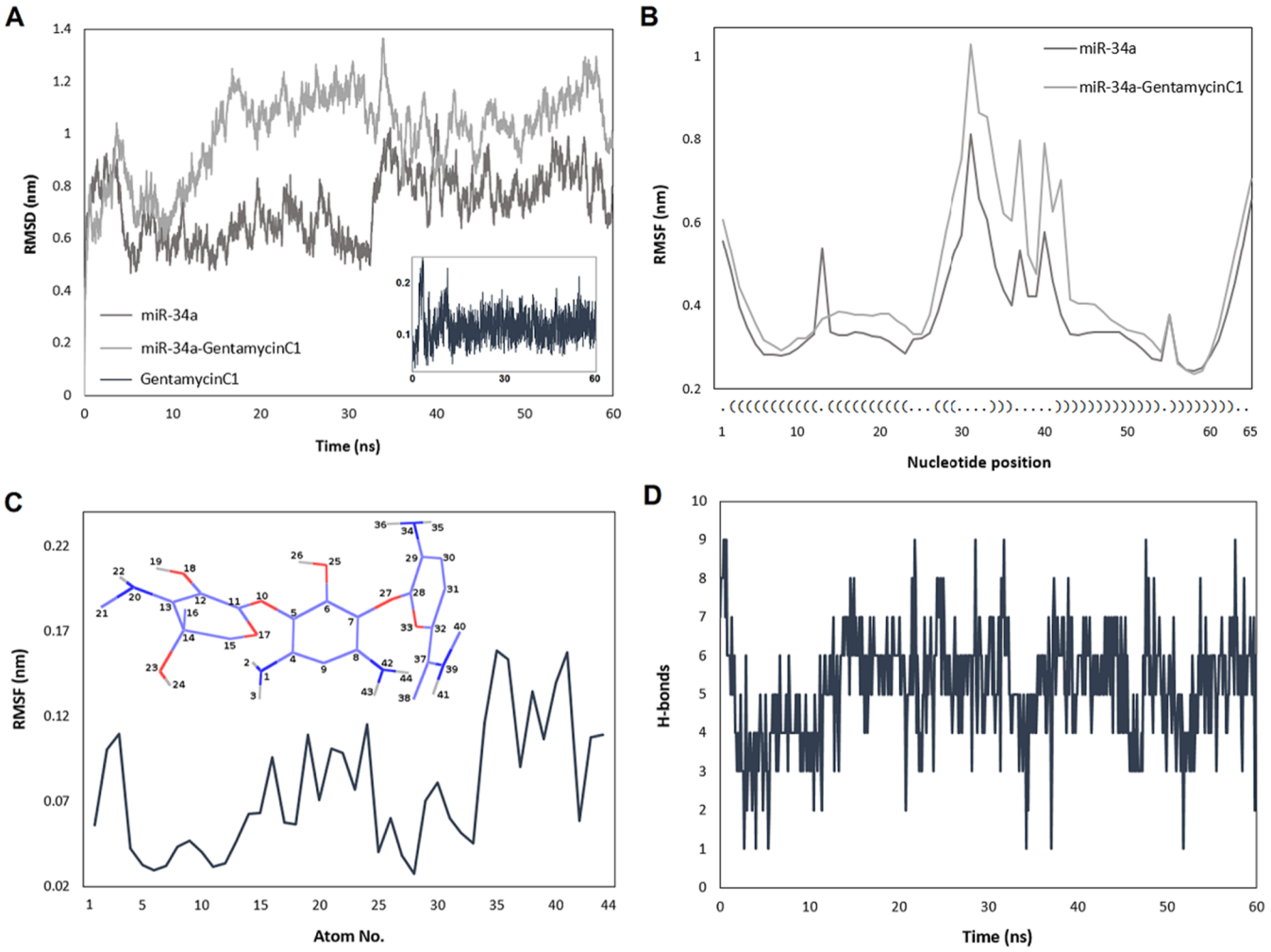

Figure 1. (A) Trends for rmsd of the free miRNA and the ligand-bound miRNA during the simulation time. rmsd for the aminoglycosidic ligand is shown in the inset; (B) RMSF along the sequence of the miRNA is illustrated with the dot-bracket representation of the RNA secondary structure; (C) RMSF for the aminoglycoside drug is shown for individual atoms as indexed in the schematic; (D) number of hydrogen bonds (H-bonds) between miR-34a and gentamycin C1, as changed during the simulation time.

each carried out in triplicate. First, the cytotoxic effects of each drug were examined in PC12 cells. Then, to assess the effect of drugs on H_2O_2-induced cytotoxicity, PC12 cells were seeded in 96-well plates (5×10^3/well) and the IC_{50} value of H_2O_2 (150 μM) and optimum concentrations of the drugs (4, 10, 20, 50, and 100 μg/mL) were considered in different modes of incubation as pretreatment, cotreatment, and post-treatment. In the pretreatment experiment, cells were incubated with the drugs for 3 h, followed by the removal of the drugs and the addition of H_2O_2 for 24 h. In cotreatment, drugs and H_2O_2 were simultaneously added for a 24 h incubation. In the post-treatment evaluation, the cells were incubated with H_2O_2 for 3 h, then they were washed, and different concentrations of the drugs were added for a 24 h incubation time.

Analysis of Apoptosis Using Annexin V-FITC/PI Double Staining Assays. To determine drug-induced apoptosis, annexin V-FITC and propidium iodate (PI) double staining assays were performed. PC12 cells were cultivated in 6-well plates for 24 h and treated with drugs alone and/or in combination. PC12 cells were collected and washed twice with PBS. Afterward, the treated and untreated cells were resuspended in 100 μL of binding buffer containing annexin V-FITC and PI, followed by fluorescence-activated cell sorting (FACS) analysis according to the manufacturer's protocol. Ten thousand events were collected for each sample, and data were acquired in list mode. Generally, in FACS analysis, annexin V +/PI− was scored as early apoptotic, and annexin V+/PI+ was considered as late apoptotic. The percentage of apoptotic cells was measured by the FACS analysis in a FACS analyzer (Attune NxT). The FlowJo 10 software (Treestar, Inc., San Carlos, CA) was used to analyze the data.

Quantitative Real-Time-PCR. PC12 cells were seeded in 6-well plates (3×10^5) and then treated with gentamycin and neomycin (4, 10, 20, 50, and 100 μg/mL) in the presence or absence of 150 μM H_2O_2. Total RNA was extracted from the PC12 cells with TRIzol reagent (Invitrogen, Carlsbard, California, USA). The RNA was reverse-transcribed into cDNA using the reverse transcription system in a 20 μL reaction according to the manufacturer's instructions. The quantitative real-time polymerase chain reaction (qRT-PCR) was performed to amplify the cDNA using the 2× SYBR Green PCR Master Mix (Bimake, Houston, TX, U.S.A.). The following primers (Invitrogen, Carlsbad, CA, U.S.A.) were used (Table 1).

Statistical Analysis. The data was presented as mean ± SD of three independent experiments. The one-way analysis of

https://doi.org/10.1021/acsomega.2c06112
ACS Omega 2023, 8, 771−781

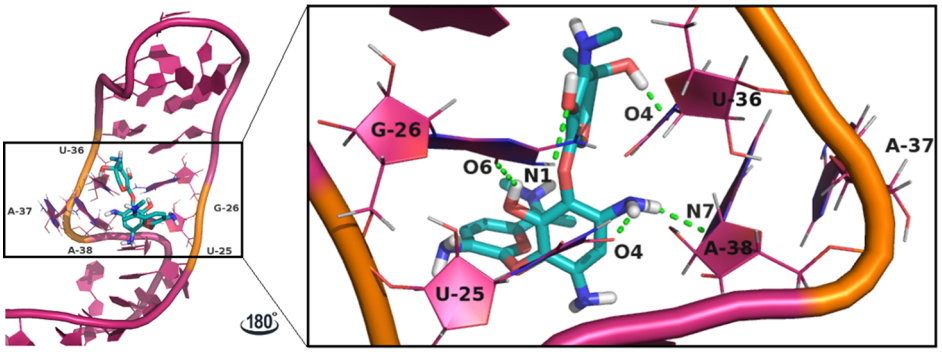

Figure 2. Illustration of H-bonding between miR-34a and gentamycin C1 for the final conformation of the RNA−drug complex. Contributing residues and their involved atoms are labeled.

variance was used for the analysis of data. The *P*-values < 0.05 were considered statistically significant.

RESULTS

Modeling the miR-34a Structure. Two secondary structural models were built for miR-34a (Figure S2). Model-1 as predicted from the raw sequence of miR-34a contained an AGGA bulge near its UAUUAG hairpin loop. The model-2 structure as predicted from database annotations included a 5′-UGUGA//UAAGGAA-3′ asymmetrical internal loop near its UAUUAG hairpin loop. The tertiary structural models built from the secondary structures are demonstrated in Figure S3. Two models showed an energy of −66.03 kcal/mol (*P*-score of −63.88) and −59.40 kcal/mol (*P*-score of −62.93), respectively.

Docking and Virtual Screening. Molecular docking was done for approved drugs against both predicted pre-miRNA-34a models, comprising a total of 58 docking experiments. As can be seen from the lowest binding energies and estimated inhibition constant values in Table 2, apramycin had the best binding with model-1 of miR-34a, while gentamycin C1 was the top-most compound hit showing the most favorable interaction with model-2. There were other promising and overlapping lead candidates between the two models, including netilmicin, neomycin C, sisomicin, framycetin, and apramycin.

Virtual screening using chemicals with structural similarity to best-binding amino sugars revealed that both lowest-energy compounds outperformed their analogues in terms of interaction with the miR-34a binding site (see Table S1 for the results of apramycin analogues and Table S2 for the results of gentamycin C1 analogues). The molecular interactions of model-1/apramycin and model-2/gentamycin C1 are depicted in Figure S4. The binding pocket was shown to be located in a narrow cleft of the miR-34a pre-element that can be readily targeted by small-molecule compounds (Figure S4).

MD Simulation. Gentamycin C1, the top-most ligand hit for model-2 of miR-34a, demonstrated an estimate of inhibition constant in the order of fM (Table 2), and it also ranked second among the best ligands of the other model (Table 2). Thus, we chose model-2 and its bound ligand for further mechanistic investigations by using MD simulations.

The system was first examined for equilibration and stability. The trajectory snapshots as illustrated in Figure S5 indicate that gentamycin C1 bound to pre-miR-34a brought about some structural fluctuations in the loop regions of the miRNA; nevertheless, it remained in its primary binding site on the miR and formed a stable complex with miR-34a. The superposition of the final conformations of free miRNA and miR complex with the aminoglycosidic drug revealed no remarkable conformational difference between the ligand-bound and ligand-free forms of pre-miR-34a (Figure S6).

The root-mean-squared deviation (rmsd) of miRNA and amino sugar became stable during the course of the simulation (Figure 1A). Additional dynamics conferred by the ligand to the miRNA is evident in the 10−35 ns interval. The gentamycin-bound miRNA then equilibrates and assumes a dynamic in a similar manner to the ligand-free miRNA. The average ± SD rmsd for free and bound miR-34a were 0.719 ± 0.12 and 1.003 ± 0.16 nm, respectively. Equal dynamics can also be inferred from the trend for the radius of gyration during the time (Figure S7A), which shows no considerable alteration in the compactness of the RNA structure upon binding to the ligand.

The dynamic behavior of the miRNA−ligand complex in the solution environment leads it to deviate from its original static conformation defined by molecular docking. Accordingly, some contacts between the miR and the aminoglycoside are lost. However, the general trend for the number of RNA−ligand contacts, as shown in Figure S7B, indicates a stable interaction between the two molecules during the 60 ns trajectory of the simulation. RNA and gentamycin C1 interact with each other with an average of 924 contacts during the time.

The ligand dynamics was also considered and measured for the system (Figure 1A: inset). It shows a stable trend with an average ± SD rmsd of 0.115 ± 0.03 nm. All these observations show that the binding of gentamycin C1 ligand to the miR-34a pre-element would not address a substantial effect on the RNA conformation. This is expected when we consider that the pre-element is folded in a hairpin structure that is relatively rigid with a number of base pairs.

The local stability of the miRNA and the drug were then examined using root-mean-squared fluctuation (RMSF), a position-wise measure of structural dynamics. As shown in Figure 1B for the miRNA, both ligand-free and ligand-bound miR-34a systems experience the greatest fluctuations in their hairpin loop and the 3′-side bulge of their internal loop. Binding of gentamycin C1 to the miRNA induced additional fluctuation in the miR structure, as also indicated by rmsd analysis. A comparison of average ± SD RMSF for free and bound miR-34a reveals no remarkable difference between the dynamics of the two RNA states in the course of simulation (0.380 ± 0.11 vs 0.451 ± 0.17 nm, respectively).

The atomic fluctuations for the amino sugar structure of the drug gentamycin C1, as shown in Figure 1C, demonstrated the highest fluctuations for the functional groups on each of the three rings composing the compound structure, as expected.

https://doi.org/10.1021/acsomega.2c06112
ACS Omega 2023, 8, 771−781

However, this analysis shows no noticeable change in the general skeleton of the aminoglycosidic compound, implying that the binding between the RNA and the ligand remained stable during the 60 ns trajectory.

The molecular profile of drug binding was also investigated by focusing on interactions. The hydrogen bonding profile of gentamycin C1 to miR-34a through the time of simulation is plotted in Figure 1D. Averagely, 5.2 H-bonds keep the drug bound to RNA. In the final trajectory frame, there were five hydrogen bonds (Figure 2). The ligand exhibited a relatively extended conformation that could sufficiently contact the base edges of a number of RNA nucleotides, including residues U25, U26, U36, and A38. All the residues are located in the upper half of the internal loop region, close to the hairpin loop of the miR pre-element. Functional groups from the aromatic center and one of the glycoside rings of gentamycin C1 involve in the interaction with miR nucleotides. In addition, the aromatic center can form hydrophobic and stacking forces with the base rings of the miRNA, contributing high stability and affinity to the complex system.

Binding Free Energy and Decomposition. We carried out the computation of binding free energy (Table 3), as well as

Table 3. Free Energy Terms and Values for the miR-34a/Gentamycin C1 Interaction

energy components	energy (kJ/mol)
ΔE_{vdW} (van der Waals energy)	−99.207
ΔE_{ele} (electrostatic energy)	−337.686
ΔE_{MM} (MM energy)	−436.893
ΔGsol-np (nonpolar solvation energy)	−11.645
$\Delta G_{sol\text{-}polar}$ (polar solvation energy)	206.973
ΔG_{PBSA} (solvation free energy)	195.328
ΔG_{polar} (polar component of free energy)	−130.713
$\Delta G_{non\text{-}polar}$ (nonpolar component of free energy)	−110.852
$\Delta G_{binding}$ (binding free energy)	−241.565

binding energy decomposition per residue (Table S3), from the snapshots extracted from the MD trajectory. To shed light on which energy components have a greater share in the total binding affinity, different energy components (ΔE_{vdw}, ΔE_{ele}, ΔG_{PB}, and ΔG_{SA}) were carefully compared. As seen in Table 3, the polar (−130.713 kJ/mol) and nonpolar (−110.852 kJ/mol) components are of almost equal favorable contributions in binding free energy of the complex, with the role of the polar element being more evident. The overall solvation energy (195.328 kJ/mol) was unfavorable for the binding of gentamycin C1 to miR-34a; however, this was compensated by desired contributions of ionic (−337.686 kJ/mol) and hydrophobic (−99.207 kJ/mol) interactions. Therefore, the polar contributions through the electrostatic forces are considered as the main driving force in the binding mechanism. Additionally, hydrophobic interactions played a crucial role in gentamycin C1 binding to the miRNA.

To get a structural view from the energy information, the total binding energy of the drug−RNA complex was broken down into drug−residue pairs in an MM/PBSA free-energy decomposition analysis (Table S3). According to this analysis, there were several nucleotides of miR-34a with large negative free-energy contributions in binding to gentamycin C1. The binding mode of the drug with the key residues is illustrated in Figure 2. As shown in Table S3, the binding site consists of residues U25, G26, U36, A37, and A38, as also shown in Figure 2 of the hydrogen bonding profile. There were also additional residues with favorable profiles which may contribute to the nonpolar component of $\Delta G_{binding}$. Accordingly, it can be concluded that the structure of the miR/ligand complex is stabilized by the shared contribution of both polar and nonpolar interactions as the fundamental forces.

Bottom-Up Lead Identification. Informa compared the structural motifs in miR-34a to the motifs in its database of annotated RNA motif−ligand interactions to generate lead compounds for our miR of interest. The output included the lead small molecules for the motifs in the miRNA and the fitness score of the predicted RNA−ligand interaction. Along with fitness, the loop nucleotides with closing base pairs (as opposed to those without closing base pairs) were considered in the ligand-motif search. Accordingly, four compounds were picked, which are proposed as potential miR-34a maturation inhibitors, in terms of binding affinity and/or miR-type selectivity (Figure S8).

Along with the structure, mechanism, and interaction studies, we also took the availability and cost issues into consideration. Thus, we proceeded to the experimental phase of the study with the two top compounds in a priority list (Table S4).

Effects of Gentamycin and Neomycin on the H_2O_2-Induced Cytotoxicity in PC12 Cells. As shown in Figure 3A,

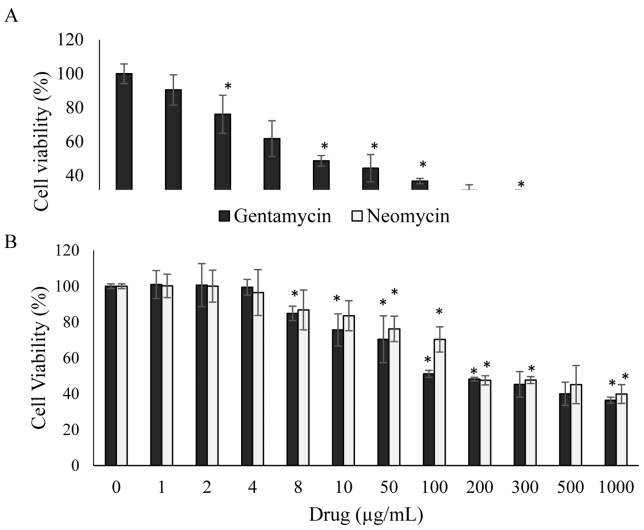

Figure 3. Cytotoxic effects of H_2O_2, gentamycin, and neomycin on PC12 cells. PC12 cells were treated with H_2O_2 (A), gentamycin, and neomycin (B) for 24 h, and the viability of cells was measured by the MTT assay. *p < 0.05, compared with the control group. All experiments were performed in triplicate, all data are expressed as the mean ± SD.

the viability of H_2O_2-treated PC12 cells decreased in a dose-dependent manner. The IC_{50} of H_2O_2 was calculated as 150 μM, which was used for further procedures. The exposure of PC12 cells to gentamycin and neomycin (1−1000 μg/mL) showed a dose-dependent reduction in the growth of PC12 cells (Figure 3B). However, increasing the concentration of drugs by up to 4 μg/mL did not show any change in the viability of the cells (Figure 3B).

Combination treatment with gentamycin/neomycin (4−100 μg/mL) and H_2O_2 (150 μM) led to an increase in the viability of cells compared to H_2O_2-treated cells. A combination of gentamycin/neomycin (4 μg/mL) and H_2O_2 (150 μM) augmented the proliferation of PC12 cells by about 81.26/

https://doi.org/10.1021/acsomega.2c06112
ACS Omega 2023, 8, 771−781

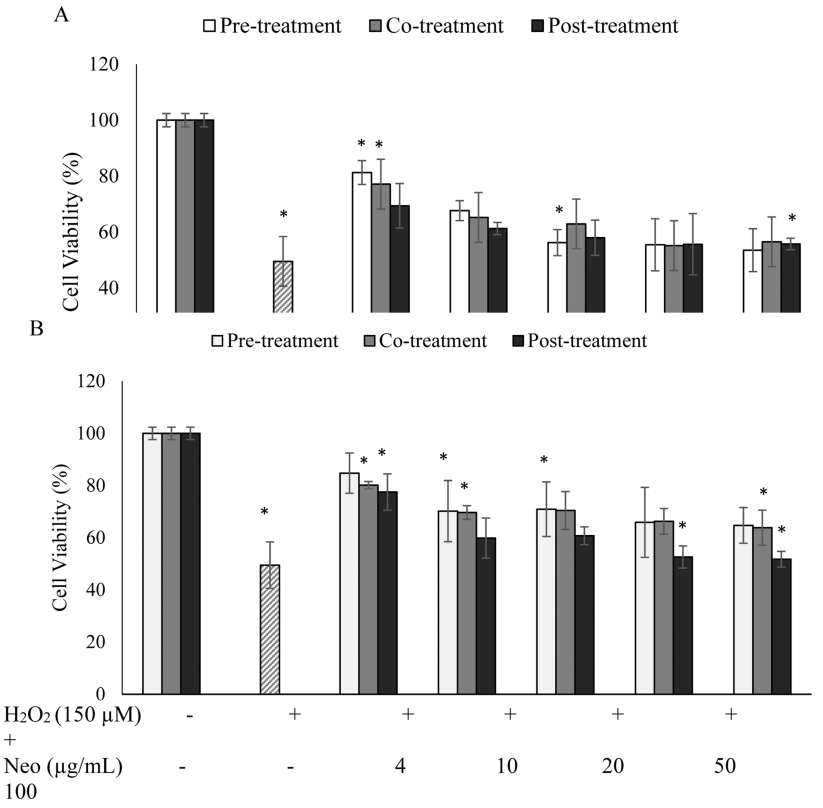

Figure 4. Effects of combination treatment of gentamycin and neomycin with H_2O_2 on the viability of PC12 cells. Gentamycin (A) and neomycin (B) at 4, 10, 20, 50, and 100 μg/mL in combination with 150 μM H_2O_2 as pre-, co-, and post-treatment were used, and the viability of PC12 cells was assayed after 24 h incubation by using the MTT assay. *$p < 0.05$, compared with the control group. All experiments were performed in triplicate; all data are expressed as the mean ± SD.

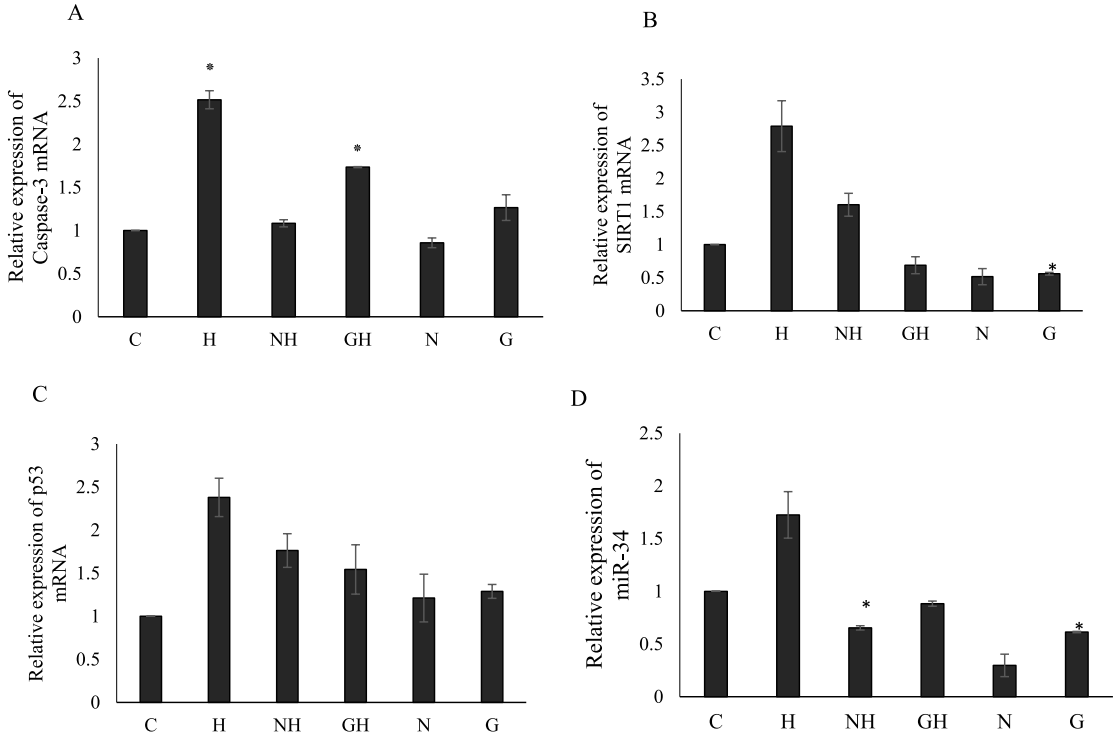

Figure 5. Expression of caspase-3, SIRT1, p53, and miR-34 in PC12 cells exposed to H_2O_2 (150 μM), gentamycin (4 μg/mL), and neomycin (4 μg/mL) alone and in combination. PC12 cells treated with H (H_2O_2), G (gentamycin, 4), N (neomycin), GH (gentamycin + H_2O_2), and NH (neomycin + H_2O_2) relative to untreated cells (C; control) and the expression of caspase-3 (A), SIRT1 (B), p53 (C), and miR-34 (D) was measured via the qRT-PCR method. *$p < 0.05$, compared with the control group. All experiments were performed in triplicate.

https://doi.org/10.1021/acsomega.2c06112
ACS Omega 2023, 8, 771−781

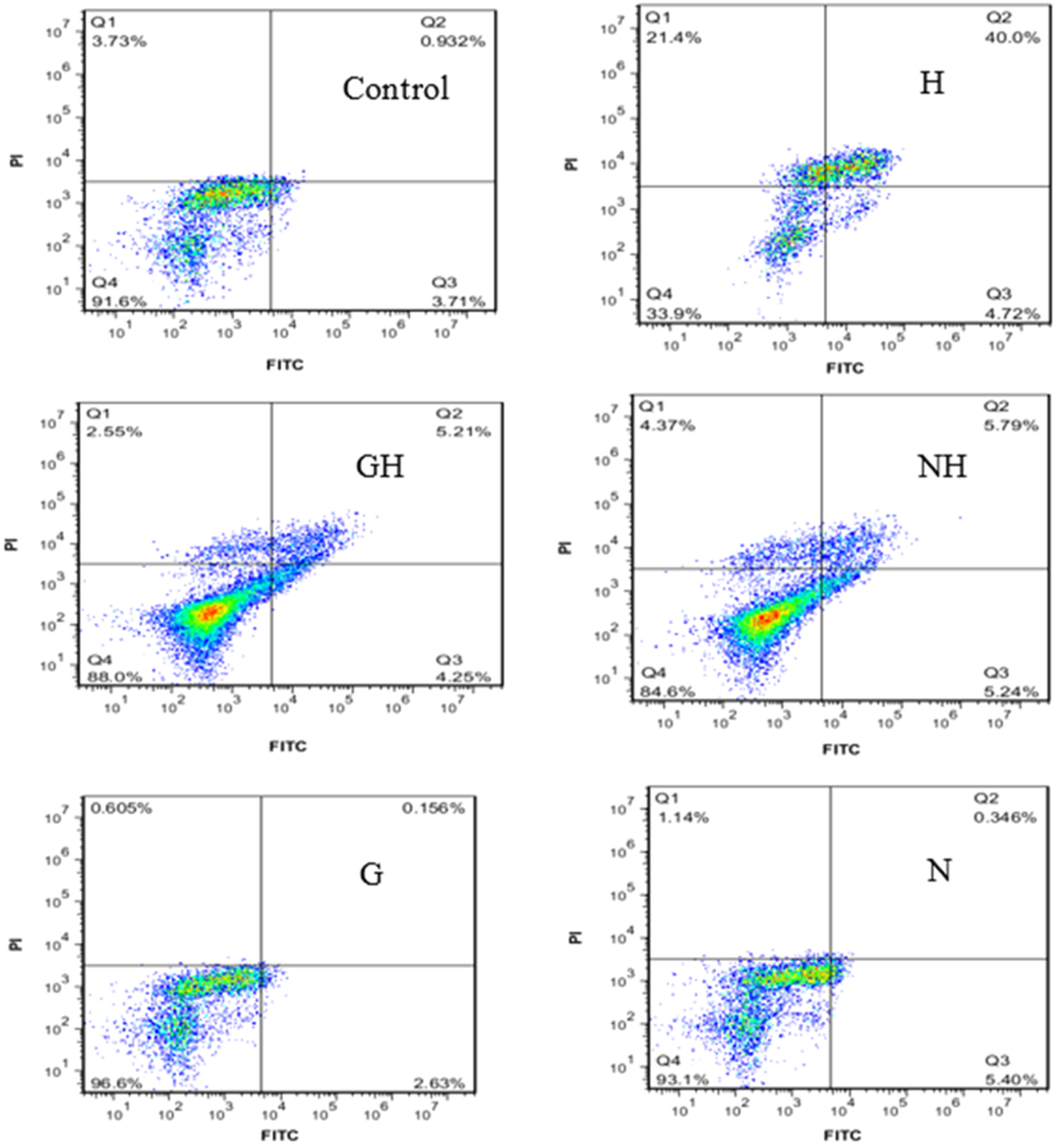

Figure 6. FITC−annexin V/PI flow cytometry analysis of PC12 cells after treatment with H (H_2O_2), G (gentamycin; 4 μg/mL), N (neomycin; 4 μg/mL), GH [gentamycin (4 μg/mL) + H_2O_2], and NH [neomycin (4 μg/mL) + H_2O_2] for 24 h. All experiments were performed in triplicate.

84.75%, 77.13/80.17%, and 69.37/77.52%, respectively, as pretreatment, cotreatment, and post-treatment compared to H_2O_2-treated cells with a nearly 50% viability (Figure 4A,B). Owing to the higher effectiveness, the pretreatment of gentamycin/neomycin (4 μg/mL) and H_2O_2 (150 μM) was used for further experiments.

Effects of Gentamycin and Neomycin on the mRNA Expression. To evaluate the underlying cytotoxic effect of H_2O_2, the expression of some key genes involved in the apoptosis pathway was evaluated in treated and untreated PC12 cells. According to Figure 5A, H_2O_2 (150 μM) led to an increased expression of caspase-3 to nearly 2.5-fold, while pretreatment with gentamycin (4 μg/mL) and neomycin (4 μg/mL) increased the expression of caspase-3 to about 1.73 and 1.1, respectively. The expression of SIRT1 was increased to 2.8-fold in the presence of H_2O_2 and decreased to about 1.1 and 1.6, in gentamycin/H_2O_2- and neomycin/H_2O_2-treated cells, respectively (Figure 5B). As indicated in Figure 5C, pretreatment of H_2O_2-treated PC12 cells with gentamycin and neomycin (4 μg/mL) exposure decreased the mRNA level of p53 to nearly 1.5-

https://doi.org/10.1021/acsomega.2c06112
ACS Omega 2023, 8, 771−781

and 1.8-fold cells compared to H_2O_2-treated cells (2.4 fold). The expression of proapoptotic miR-34 was upregulated in H_2O_2-treated cells (1.7 fold) and was downregulated in PC12 cells treated with gentamycin/H_2O_2 and neomycin/H_2O_2 to about 0.9- and 0.6-fold, respectively (Figure 5D). The results implied that gentamycin and neomycin modulating the expression of cell proliferation and apoptosis factors including p53, SIRT-1, caspase-3, and miR-34 could augment the growth of PC12 exposed to H_2O_2.

Effects of Gentamycin and Neomycin on the H_2O_2-Induced Apoptosis in PC12 Cells. Based on the annexin V-affinity of phosphatidylserine on the outer membrane, apoptotic cells can be distinguished from annexin V-negative living cells by using flow cytometric procedures. When PC12 cells were treated with H_2O_2 (150 μM), the percentages of late apoptotic and necrotic cells increased by about 40 and 21.4% with no obvious early apoptosis compared to untreated control cells (Figure 6). Furthermore, as shown in Figure 6, the treatment of PC12 cells with gentamycin/neomycin (4 μg/mL) had no significant effect on the early and late apoptotic population, while pretreatment using gentamycin/H_2O_2 (4 μg/mL/150 μM) and neomycin/H_2O_2 (4 μg/mL/150 μM) decreased the viability of late apoptotic/necrotic cells to 5.21/2.55% and 5.79/4.37%, respectively. Data clearly indicated that H_2O_2 treatment is associated with the induction of apoptosis and a combination of gentamycin- or neomycin-protected PC12 cells against the cytotoxicity of H_2O_2.

DISCUSSION

Although suppressing miRNAs' function by using oligonucleotide or peptide antimiRs allows them to achieve target specificity in vivo, their usage may accompany challenges such as poor cellular delivery and the manifestation of off-target effects.[13] Thus, we considered the design of small-molecule inhibitors for miR-34a function.[23−25] For this purpose, the computer-aided rational drug design approach was adopted as it has been a successful method for proposing anti-miR compounds against several miRNA types in various diseases.[25,33−38] The top lead compounds were then tested on oxidatively injured PC12 cells as a neuropathological cell model.

Aminoglycoside-based therapeutics demonstrate great potential as inhibitors against the miRNA biogenesis pathway. This class of compounds bind to the stem-loop region and nearby bulges and occludes the binding site of the Dicer enzyme, this way suppressing the miRNA processing to maturation.[39] The approach applied here represents an application of drug repositioning, as most aminoglycosides are already proposed as antibiotic drugs approved by relevant administrations for clinical use. Such an approach eliminates the need for the evaluation of inhibitory molecules in terms of pharmacokinetics and cytotoxicity. We only considered a pharmacokinetic analysis using admetSAR[40] to predict the permeability of the repurposed drugs through cerebrovascular endothelial cells. This analysis showed a 98.2% probability of BBB permeability for gentamycin C1, implying its convenient delivery to the brain in in vivo or patient-level treatments of ischemic stroke.

In addition to the rational design, we considered high-specificity leads for miR-34a from an experiment-based data repository. In this strategy, the fitness of RNA motif−ligand interaction provides a means for the small molecule to dictate its ideal RNA target; that is, it could be deemed as a target-agnostic and bottom-up design approach. The advantage of this method is the integration of both affinity and selectivity features in the fitness to score the miRNA−small ligand interactions.[26,31] Interestingly, there is a high structural similarity between motif-733 and gentamycin C1 (Figures S1 and S8), indicating that the high miR-34a binding specificity of the target-agnostic lead may also be represented by the repurposed anti-miR and gentamycin C1. Other leads with highly selective and/or strong binding to miR-34a were not assayed here due to limitations in availability or cost. Our list of leads (Table S4) is recommended as a reference for future studies to test the compounds experimentally against the miR.

Given that increased levels of oxidative stress are involved in the pathogenesis of ischemic stroke, H_2O_2 was used to induce an oxidative injury model of the disease in PC12 cells.[41−43] As indicated, H_2O_2 treatment led to decreased levels of viability and increased content of apoptosis via the induction of p53, Caspase-3, SIRT1, and miR-34, while the pretreatment of H_2O_2-induced PC12 cells with gentamycin and neomycin reduced the apoptotic/necrotic cells and modulated the levels of apoptotic factors. Thus, these amino-sugar treatments may play a pivotal role in the protection of neural cells against the apoptosis induced by stroke.

The regulatory triad axis p53/miR-34a/SIRT1 represents a positive feedback loop comprising the promotion of the miR by p53, direct suppression of SIRT1 by the miR, and inactivation of p53 by SIRT1 via deacetylation.[44−46] This pathway has also been shown in PC12 cells using miR-34a mimics/inhibitors.[47] The miRNA also modulated Bcl-2 and cytochrome C, which affected the mitochondrial outer membrane integrity.[47] However, miR-34a is under tight regulation which may be varied with different stimuli.[48] In our study, using oxidative injury preceded with gentamycin treatment, we found decreased levels of miR-34, increased levels of p53 and caspase-3 mRNAs, and decreased SIRT1 mRNA levels, compared to the untreated control. As expected, caspase-3 as a proapoptotic and downstream gene of p53 demonstrated a behavior similar to p53 in the presence of gentamycin or gentamycin/H_2O_2. However, the regulation of other factors was inconsistent with the p53/miR-34a/SIRT1 feedback loop. In general, the regulation of neuronal Sirtuins by miR-34a poses a paradoxical situation for maintaining neuronal survival and may imply an intricate balance of miR-34a levels and SIRT1 levels/activity to maintain neuronal survival and function.[18] In a perturbation analysis of miR-34a/p53/SIRT1 in animal Huntington's disease models, the observed changes did not reflect the known interactions between these factors. This was attributed to possible outside factors modulating this triad pathway.[49] Specifically, in our molecular modeling study, gentamycin demonstrated a direct and strong interaction with miR-34a and may exert its modulatory effect on PC12 cellular apoptosis via this binding. Other feedback loops which involve miR-34 can be affected by this interaction and result in the downregulation of the miRNA and its consequent reduced apoptosis even with the unexpected changes observed in p53/SIRT1.[48] The dual role of SIRT1 may also explain our observations. Though known as an antiapoptotic factor, there is accumulating evidence of the multifaceted modulation of SIRT1 in inflammation and tumorigenic conditions.[50−52] In fact, SIRT1 might play a multifaceted role in different tissue contexts depending on the spatiotemporal distribution of its upstream and downstream factors.[51] Most of the research on cerebrovascular pathology supports a neuroprotective role for SIRT1;[53−55] nevertheless, the ischemic insult has unanticipatedly not been ameliorated by SIRT1 in some studies.[56,57] Due to the complicated and elusive

https://doi.org/10.1021/acsomega.2c06112
ACS Omega 2023, 8, 771−781

nature of the network involved in eliciting apoptosis in neural cells, it is also challenging to justify why pretreated neomycin outperformed gentamycin in the negative regulation of miRNA expression.

CONCLUSIONS

Gentamycin enhanced cell viability and ameliorated cell death in the PC12 model of stroke. Our findings will help to further understand how the suppression of miR-34a in neural tissue affects cell viability and BBB function poststroke. Before clinical tests, a comprehensive appraisal of the potential of the introduced small inhibitory compounds against stroke outcomes at the molecular, cellular, and physiological levels is essential. Accordingly, conducting in vivo experiments is suggested to examine the efficacy of the designed inhibitors under stroke pathophysiological conditions.

ASSOCIATED CONTENT

Supporting Information

The Supporting Information is available free of charge at https://pubs.acs.org/doi/10.1021/acsomega.2c06112.

Aminoglycoside compounds, secondary and tertiary structures for miR-34a, docking experiments, lead compound structure, structure-based screening results, and ranked list of hit compounds for exploring anti-miR-34a lead ligands (PDF)

AUTHOR INFORMATION

Corresponding Authors

Soraya Sajadimajd − *Department of Biology, Faculty of Science, Razi University, Kermanshah 67144-14971, Iran*; Email: s.sajadi@razi.ac.ir

Hossein Derakhshankhah − *Pharmaceutical Sciences Research Center, Health Institute, Kermanshah University of Medical Sciences, Kermanshah 6715847141, Iran; USERN Office, Kermanshah University of Medical Sciences, Kermanshah 6715847141, Iran;* orcid.org/0000-0002-0951-2729; Email: derakhshankhah.hossein@gmail.com

Authors

Zhila Izadi − *Pharmaceutical Sciences Research Center, Health Institute, Kermanshah University of Medical Sciences, Kermanshah 6715847141, Iran; USERN Office, Kermanshah University of Medical Sciences, Kermanshah 6715847141, Iran;* orcid.org/0000-0002-4546-5202

Ebrahim Barzegari − *Medical Biology Research Center, Health Technology Institute, Kermanshah University of Medical Sciences, Kermanshah 6715847141, Iran;* orcid.org/0000-0002-4412-6129

Amin Iranpanah − *Pharmaceutical Sciences Research Center, Health Institute, Kermanshah University of Medical Sciences, Kermanshah 6715847141, Iran; USERN Office, Kermanshah University of Medical Sciences, Kermanshah 6715847141, Iran*

Complete contact information is available at: https://pubs.acs.org/10.1021/acsomega.2c06112

Notes

The authors declare no competing financial interest.

ACKNOWLEDGMENTS

This work was supported by the National Institute for Medical Research Development of the Islamic Republic of Iran (NIMAD, grant number: 984499) and the Kermanshah University of Medical Sciences, Kermanshah, Iran.

REFERENCES

(1) GBD 2015 Neurological Disorders Collaborator Group. Global, regional, and national burden of neurological disorders during 1990-2015: a systematic analysis for the Global Burden of Disease Study 2015. *Lancet Neurol.* **2017**, *16*, 877−897.

(2) Katan, M.; Luft, A. Global Burden of Stroke. *Semin. Neurol.* **2018**, *38*, 208−211.

(3) Gorelick, P. B. The global burden of stroke: persistent and disabling. *Lancet Neurol.* **2019**, *18*, 417−418.

(4) Donkor, E. S. Stroke in the 21st century: a snapshot of the burden, epidemiology, and quality of life. *Stroke Res. Treat.* **2018**, *2018*, 3238165.

(5) Hankey, G. J. Stroke. *Lancet* **2017**, *389*, 641−654.

(6) Feske, S. K. Ischemic Stroke. *Am. J. Med.* **2021**, *134*, 1457.

(7) Mo, Y.; Xu, W.; Fu, K.; Chen, H.; Wen, J.; Huang, Q.; Guo, F.; Mo, L.; Yan, J. The dual function of microglial polarization and its treatment targets in ischemic stroke. *Front. Neurol.* **2022**, *13*, 921705.

(8) Sacco, R. L.; Kasner, S. E.; Broderick, J. P.; Caplan, L. R.; Connors, J. J.; Culebras, A.; Elkind, M. S. V.; George, M. G.; Hamdan, A. D.; Higashida, R. T.; et al. An Updated Definition of Stroke for the 21st Century. a statement for healthcare professionals from the American Heart Association/American Stroke Association. *Stroke* **2013**, *44*, 2064−2089.

(9) Radak, D.; Resanovic, I.; Isenovic, E. R. Link between oxidative stress and acute brain ischemia. *Angiology* **2014**, *65*, 667−676.

(10) Dixon, S. J.; Stockwell, B. R. The role of iron and reactive oxygen species in cell death. *Nat. Chem. Biol.* **2014**, *10*, 9−17.

(11) Rodrigo, R.; Fernandez-Gajardo, R.; Gutierrez, R.; Matamala, J. M.; Carrasco, R.; Miranda-Merchak, A.; Feuerhake, W. Oxidative stress and pathophysiology of ischemic stroke: novel therapeutic opportunities. *CNS Neurol. Disord.: Drug Targets* **2013**, *12*, 698−714.

(12) Yuan, L.; Chen, W.; Xiang, J.; Deng, Q.; Hu, Y.; Li, J. Advances of circRNA-miRNA-mRNA regulatory network in cerebral ischemia/reperfusion injury. *Exp. Cell Res.* **2022**, *419*, 113302.

(13) Rupaimoole, R.; Slack, F. J. MicroRNA therapeutics: towards a new era for the management of cancer and other diseases. *Nat. Rev. Drug Discov.* **2017**, *16*, 203−222.

(14) Deng, Y.; Huang, P.; Zhang, F.; Chen, T. Association of MicroRNAs With Risk of Stroke: A Meta-Analysis. *Front. Neurol.* **2022**, *13*, 865265.

(15) Tsermpini, E. E.; Kalogirou, C. I.; Kyriakopoulos, G. C.; Patrinos, G. P.; Stathopoulos, C. miRNAs as potential diagnostic biomarkers and pharmacogenomic indicators in psychiatric disorders. *Pharmacogenomics J.* **2022**, *22*, 211−222.

(16) Li, W. J.; Wang, Y.; Liu, R.; Kasinski, A. L.; Shen, H.; Slack, F. J.; Tang, D. G. MicroRNA-34a: Potent Tumor Suppressor, Cancer Stem Cell Inhibitor, and Potential Anticancer Therapeutic. *Front. Cell Dev. Biol.* **2021**, *9*, 640587.

(17) Raucci, A.; Macrì, F.; Castiglione, S.; Badi, I.; Vinci, M. C.; Zuccolo, E. MicroRNA-34a: the bad guy in age-related vascular diseases. *Cell. Mol. Life Sci.* **2021**, *78*, 7355−7378.

(18) Chua, C. E. L.; Tang, B. L. miR-34a in Neurophysiology and Neuropathology. *J. Mol. Neurosci.* **2019**, *67*, 235−246.

(19) Bukeirat, M.; Sarkar, S. N.; Hu, H.; Quintana, D. D.; Simpkins, J. W.; Ren, X. MiR-34a regulates blood-brain barrier permeability and mitochondrial function by targeting cytochrome c. *J. Cereb. Blood Flow Metab.* **2016**, *36*, 387−392.

(20) Sarkar, S.; Jun, S.; Rellick, S.; Quintana, D. D.; Cavendish, J. Z.; Simpkins, J. W. Expression of microRNA-34a in Alzheimer's disease brain targets genes linked to synaptic plasticity, energy metabolism, and resting state network activity. *Brain Res.* **2016**, *1646*, 139−151.

(21) Alluri, H.; Stagg, H. W.; Wilson, R. L.; Clayton, R. P.; Sawant, D. A.; Koneru, M.; Beeram, M. R.; Davis, M. L.; Tharakan, B. Reactive oxygen species-caspase-3 relationship in mediating blood-brain barrier endothelial cell hyperpermeability following oxygen-glucose deprivation and reoxygenation. *Microcirculation* **2014**, *21*, 187−195.
(22) Ren, X.; Engler-Chiurazzi, E. B.; Russell, A. E.; Sarkar, S. N.; Rellick, S. L.; Lewis, S.; Corbin, D.; Clapper, J.; Simpkins, J. W. MiR-34a and stroke: assessment of non-modifiable biological risk factors in cerebral ischemia. *Neurochem. Int.* **2019**, *127*, 73−79.
(23) Nahar, S.; Ranjan, N.; Ray, A.; Arya, D. P.; Maiti, S. Potent inhibition of miR-27a by neomycin−bisbenzimidazole conjugates. *Chem. Sci.* **2015**, *6*, 5837−5846.
(24) Wen, D.; Danquah, M.; Chaudhary, A. K.; Mahato, R. I. Small molecules targeting microRNA for cancer therapy: Promises and obstacles. *J. Controlled Release* **2015**, *219*, 237−247.
(25) Ghosh, A.; Degyatoreva, N.; Kukielski, C.; Story, S.; Bhaduri, S.; Maiti, K.; Nahar, S.; Ray, A.; Arya, D. P.; Maiti, S. Targeting miRNA by tunable small molecule binders: peptidic aminosugar mediated interference in miR-21 biogenesis reverts epithelial to mesenchymal transition. *MedChemComm* **2018**, *9*, 1147−1154.
(26) Velagapudi, S. P.; Gallo, S. M.; Disney, M. D. Sequence-based design of bioactive small molecules that target precursor microRNAs. *Nat. Chem. Biol.* **2014**, *10*, 291−297.
(27) Parisien, M.; Major, F. The MC-Fold and MC-Sym pipeline infers RNA structure from sequence data. *Nature* **2008**, *452*, 51−55.
(28) Van Der Spoel, D.; Lindahl, E.; Hess, B.; Groenhof, G.; Mark, A. E.; Berendsen, H. J. GROMACS: fast, flexible, and free. *J. Comput. Chem.* **2005**, *26*, 1701−1718.
(29) Sousa da Silva, A. W.; Vranken, W. F. ACPYPE - AnteChamber PYthon Parser interfacE. *BMC Res. Notes* **2012**, *5*, 367.
(30) Kumari, R.; Kumar, R.; Lynn, A. g_mmpbsa–a GROMACS tool for high-throughput MM-PBSA calculations. *J. Chem. Inf. Model.* **2014**, *54*, 1951−1962.
(31) Disney, M. D.; Winkelsas, A. M.; Velagapudi, S. P.; Southern, M.; Fallahi, M.; Childs-Disney, J. L. Inforna 2.0: A Platform for the Sequence-Based Design of Small Molecules Targeting Structured RNAs. *ACS Chem. Biol.* **2016**, *11*, 1720−1728.
(32) Vistica, D. T.; Skehan, P.; Scudiero, D.; Monks, A.; Pittman, A.; Boyd, M. R. Tetrazolium-based assays for cellular viability: a critical examination of selected parameters affecting formazan production. *Cancer Res.* **1991**, *51*, 2515−2520.
(33) Bose, D.; Jayaraj, G.; Suryawanshi, H.; Agarwala, P.; Pore, S. K.; Banerjee, R.; Maiti, S. The tuberculosis drug streptomycin as a potential cancer therapeutic: inhibition of miR-21 function by directly targeting its precursor. *Angew. Chem., Int. Ed. Engl.* **2012**, *51*, 1019−1023.
(34) Chen, X.; Xie, B.; Cao, L.; Zhu, F.; Chen, B.; Lv, H.; Fan, X.; Han, L.; Bie, L.; Cao, X.; et al. Direct binding of microRNA-21 pre-element with Regorafenib: An alternative mechanism for anti-colorectal cancer chemotherapy? *J. Mol. Graphics Modell.* **2017**, *73*, 48−53.
(35) Jayaraj, G. G.; Nahar, S.; Maiti, S. Nonconventional chemical inhibitors of microRNA: therapeutic scope. *Chem. Commun.* **2015**, *51*, 820−831.
(36) Shi, Z.; Zhang, J.; Qian, X.; Han, L.; Zhang, K.; Chen, L.; Liu, J.; Ren, Y.; Yang, M.; Zhang, A.; et al. AC1MMYR2, an inhibitor of dicer-mediated biogenesis of Oncomir miR-21, reverses epithelial-mesenchymal transition and suppresses tumor growth and progression. *Cancer Res.* **2013**, *73*, 5519−5531.
(37) Sinoy, S.; Fayaz, S. M.; Charles, K. D.; Suvanish, V. K.; Kapfhammer, J. P.; Rajanikant, G. K. Amikacin Inhibits miR-497 Maturation and Exerts Post-ischemic Neuroprotection. *Mol. Neurobiol.* **2017**, *54*, 3683−3694.
(38) Thomas, M.; Deiters, A. MicroRNA miR-122 as a therapeutic target for oligonucleotides and small molecules. *Curr. Med. Chem.* **2013**, *20*, 3629−3640.
(39) Tripp, V. T.; McKenna, J. R.; Young, D. D. Approaches to the modulation of miRNA maturation. *Methods Mol. Biol.* **2014**, *1095*, 27−58.
(40) Cheng, F.; Li, W.; Zhou, Y.; Shen, J.; Wu, Z.; Liu, G.; Lee, P. W.; Tang, Y. admetSAR: a comprehensive source and free tool for assessment of chemical ADMET properties. *J. Chem. Inf. Model.* **2012**, *52*, 3099−3105.
(41) Chu, Q.; Yu, L.; Zheng, Z.; Chen, M.; Hua, Z.; Hang, M.; Li, Y.; Li, X.; Liu, Y.; Yang, Y.; et al. Apios americana Medik flowers extract protects PC12 cells against H_2O_2 induced neurotoxicity via regulating autophagy. *Food Chem. Toxicol.* **2019**, *124*, 231−238.
(42) Rong, Z. T.; Gong, X. J.; Sun, H. B.; Li, Y. M.; Ji, H. Protective effects of oleanolic acid on cerebral ischemic damage in vivo and $H_{(2)}O_{(2)}$-induced injury in vitro. *Pharm. Biol.* **2011**, *49*, 78−85.
(43) Zhang, Z.; Xu, P.; Yu, H.; Shi, L. Luteolin protects PC-12 cells from H_2O_2-induced injury by up-regulation of microRNA-21. *Biomed. Pharmacother.* **2019**, *112*, 108698.
(44) Yamakuchi, M.; Ferlito, M.; Lowenstein, C. J. miR-34a repression of SIRT1 regulates apoptosis. *Proc. Natl. Acad. Sci. U.S.A.* **2008**, *105*, 13421−13426.
(45) Li, L.; Yuan, L.; Luo, J.; Gao, J.; Guo, J.; Xie, X. MiR-34a inhibits proliferation and migration of breast cancer through down-regulation of Bcl-2 and SIRT1. *Clin. Exp. Med.* **2013**, *13*, 109−117.
(46) Mandke, P.; Wyatt, N.; Fraser, J.; Bates, B.; Berberich, S. J.; Markey, M. P. MicroRNA-34a modulates MDM4 expression via a target site in the open reading frame. *PLoS One* **2012**, *7*, No. e42034.
(47) Lin, Q.; Mao, Y.; Song, Y.; Huang, D. MicroRNA 34a induces apoptosis in PC12 cells by reducing B cell lymphoma 2 and sirtuin 1 expression. *Mol. Med. Rep.* **2015**, *12*, 5709−5714.
(48) Rokavec, M.; Li, H.; Jiang, L.; Hermeking, H. The p53/miR-34 axis in development and disease. *J. Mol. Cell Biol.* **2014**, *6*, 214−230.
(49) Reynolds, R. H.; Petersen, M. H.; Willert, C. W.; Heinrich, M.; Nymann, N.; Dall, M.; Treebak, J. T.; Björkqvist, M.; Silahtaroglu, A.; Hasholt, L.; et al. Perturbations in the p53/miR-34a/SIRT1 pathway in the R6/2 Huntington's disease model. *Mol. Cell. Neurosci.* **2018**, *88*, 118−129.
(50) Fang, Y.; Nicholl, M. B. A dual role for sirtuin 1 in tumorigenesis. *Curr. Pharm. Des.* **2014**, *20*, 2634−2636.
(51) Fang, Y.; Nicholl, M. B. Sirtuin 1 in malignant transformation: Friend or foe? *Cancer Lett.* **2011**, *306*, 10−14.
(52) Yang, H.; Bi, Y.; Xue, L.; Wang, J.; Lu, Y.; Zhang, Z.; Chen, X.; Chu, Y.; Yang, R.; Wang, R.; et al. Multifaceted Modulation of SIRT1 in Cancer and Inflammation. *Crit. Rev. Oncog.* **2015**, *20*, 49−64.
(53) Hattori, Y.; Okamoto, Y.; Nagatsuka, K.; Takahashi, R.; Kalaria, R. N.; Kinoshita, M.; Ihara, M. SIRT1 attenuates severe ischemic damage by preserving cerebral blood flow. *Neuroreport* **2015**, *26*, 113−117.
(54) Hernández-Jiménez, M.; Hurtado, O.; Cuartero, M. I.; Ballesteros, I.; Moraga, A.; Pradillo, J. M.; McBurney, M. W.; Lizasoain, I.; Moro, M. A. Silent information regulator 1 protects the brain against cerebral ischemic damage. *Stroke* **2013**, *44*, 2333−2337.
(55) Wei, G.; Wang, J.; Wu, Y.; Zheng, X.; Zeng, Y.; Li, Y.; Chen, X. Sirtuin 1 alleviates neuroinflammation-induced apoptosis after traumatic brain injury. *J. Cell. Mol. Med.* **2021**, *25*, 4478−4486.
(56) Sansone, L.; Reali, V.; Pellegrini, L.; Villanova, L.; Aventaggiato, M.; Marfe, G.; Rosa, R.; Nebbioso, M.; Tafani, M.; Fini, M.; et al. SIRT1 silencing confers neuroprotection through IGF-1 pathway activation. *J. Cell. Physiol.* **2013**, *228*, 1754−1761.
(57) Esmayel, I. M.; Hussein, S.; Gohar, E. A.; Ebian, H. F.; Mousa, M. M. Plasma levels of sirtuin-1 in patients with cerebrovascular stroke. *Neurol. Sci.* **2021**, *42*, 3843−3850.

https://doi.org/10.1021/acsomega.2c06112
ACS Omega 2023, 8, 771−781